

Estimation of the knee joint angle from surface electromyographic signals for active control of leg prostheses

Alberto L Delis^{1,2}, João L A Carvalho^{1,3}, Adson F da Rocha¹,
Renan U Ferreira¹, Suéila S Rodrigues³ and Geovany A Borges¹

¹ Department of Electrical Engineering, University of Brasília, Brasília-DF, Brazil

² Medical Biophysics Center, University of Oriente, Santiago de Cuba, Cuba

³ UNB-Gama Faculty, University of Brasília, Gama-DF, Brazil

E-mail: gaborges@ene.unb.br

Received 26 March 2009, accepted for publication 14 July 2009

Published 6 August 2009

Online at stacks.iop.org/PM/30/931

Abstract

The surface electromyographic (SEMG) signal is very convenient for prosthesis control because it is non-invasively acquired and intrinsically related to the user's intention. This work presents a feature extraction and pattern classification algorithm for estimation of the intended knee joint angle from SEMG signals acquired using two sets of electrodes placed on the upper leg. The proposed algorithm uses a combination of time-domain and frequency-domain approaches for feature extraction (signal amplitude histogram and auto-regressive coefficients, respectively), a self-organizing map for feature projection and a Levenberg–Marquardt multi-layer perceptron neural network for pattern classification. The new algorithm was quantitatively compared with the method proposed by Wang *et al* (2006 *Med. Biol. Eng. Comput.* **44** 865–72), which uses wavelet packet feature extraction, principal component analysis and a multi-layer perceptron neural classifier. The proposed method provided lower error-to-signal percentage and peak error amplitudes, higher correlation and fewer error events. The algorithm presented in this work may be useful as part of a myoelectric controller for active leg prostheses designed for transfemoral amputees.

Keywords: electromyographic signals, prosthesis control, feature extraction, dimensionality reduction, neural networks, microcontrolled instrumentation

(Some figures in this article are in colour only in the electronic version)

1. Introduction

Surface electromyographic (SEMG) signals provide a non-invasive tool for investigating the properties of skeletal muscles (Sommerich *et al* 2000). SEMG signals may be used not only for monitoring muscle behavior during rehabilitation programs (Monseni-Bendpei *et al* 2000), but also for mechanical control of prostheses (Englehart and Hudgins 2003). The SEMG signal is very convenient for prosthesis control because it is intrinsically related to the user's intention (Hudgins *et al* 1993). In such an application, it is important to be able to correctly predict which movement is planned by the user. A myoelectric control algorithm should be capable of learning the muscular activation patterns that are used in natural form for typical movements. It also needs robustness against variations in conditions during operation, and the response time cannot cause delays that are noticeable to the user (Fukuda *et al* 2003).

The central component of a pattern-recognition-based myoelectric control algorithm is the neural network classifier, which must be capable of learning relationships between input SEMG signals and desired control outputs. Increasing the number of SEMG channels that are acquired and processed may provide the user with higher accuracy in controlling the intensity of the contraction (Englehart *et al* 2001). However, as the number of inputs increases, the complexity of the network structure grows exponentially, which significantly increases the convergence time. Data pre-processing is typically used for reducing the amount of data analyzed by the neural classifier. A common approach is to extract parameters from the data, such as time-domain features (e.g. mean absolute value, waveform length, number of zero crossings) (Kelly *et al* 1990, Hudgins *et al* 1993), spectral parameters (e.g. auto-regressive model) (Huang *et al* 2005, Hargrove *et al* 2008), time-frequency coefficients (e.g. short-time Fourier transform) (Englehart *et al* 2001) and/or time-scale coefficients (e.g. discrete wavelet transform, wavelet packet decomposition) (Englehart *et al* 2001, Chu *et al* 2005, Wang *et al* 2006). Further data reduction may be achieved using a feature projection stage between pre-processing and classification (Englehart *et al* 2001, Chu *et al* 2005, Wang *et al* 2006). This approach eliminates redundant information, which speeds up the training process. It may also help mapping the data into small and well-separated clusters, by absorbing signal variations and noise present in the data's original vector space.

The data processing and classification techniques discussed above have been successfully used for myoelectric control by several groups. Kelly *et al* (1990) proposed an algorithm capable of discriminating between four motions of elbow and wrist joints from SEMG patterns measured from one pair of electrodes, using a Hopfield neural network for time-domain feature extraction, followed by a two-layer perceptron neural classifier. Englehart *et al* (2001) designed an algorithm for dexterous and natural myoelectric control of powered upper limbs using a linear discriminant analysis (LDA) classifier, after principal components analysis (PCA) dimensionality reduction on a wavelet-based feature set. Chu *et al* (2005) presented a pattern recognition algorithm for the control of a multifunction myoelectric hand, using the wavelet packet transform for feature extraction, a multi-layer neural network classifier and a linear–nonlinear feature projection composed of PCA and self-organizing feature maps, respectively. Huang *et al* (2005) designed a classification scheme based on Gaussian mixture models for myoelectric control of upper limb prostheses, using feature extraction based on time-domain statistics, auto-regressive (AR) coefficients and the root mean square of the signal. Wang *et al* (2006) proposed an algorithm capable of discriminating between four types of hand and forearm movements, using wavelet packet feature extraction and PCA feature projection. Zhao *et al* (2006) designed a control algorithm capable of recognizing six different hand motion patterns, using a multi-layer perceptron neural network classifier and feature

extraction based on sample entropy, time-domain filtering and wavelet transform coefficients. Hargrove *et al* (2008) used a combination of time-domain features and AR coefficients with a LDA classifier to determine the effect of electrode displacements on pattern classification accuracy, and to design a classifier training strategy to address this issue.

Despite great successes in decoding discrete movements such as individual finger flexion or extension, the matter of continuously predicting joint angles using SEMG is comparatively underdeveloped (Smith *et al* 2008). This work presents a feature extraction and pattern classification algorithm for estimating the intended knee joint angle from a two-channel SEMG signal, acquired using surface electrodes placed on the upper leg. This algorithm was designed for myoelectric control of an active transfemoral prosthesis (Cascão Jr *et al* 2005, Rodrigues *et al* 2006), as an improvement to the algorithm proposed by Ferreira *et al* (2005). The algorithm by Ferreira *et al* consisted in using the AR model for feature extraction, and a Levenberg–Marquardt (LM) multi-layer perceptron neural network (Hagan and Menhaj 1994) for pattern classification. The proposed method improves the feature extraction stage by using a combination of spectral and temporal domain approaches—AR coefficients (Huang *et al* 2005, Hargrove *et al* 2008) and signal amplitude histogram (Zardoshti-Kermani *et al* 1995, Liu *et al* 2007), respectively—and by incorporating a feature projection stage, using a self-organizing map (SOM) (Kohonen 2001). The incorporated Kohonen network reduces the dimensionality of the data at the input of the LM neural classifier, by mapping all the AR and histogram coefficients into a two-dimensional vector space (Chu *et al* 2005). The new algorithm was quantitatively compared to its original version (Ferreira *et al* 2005) and to a different method from the literature (Wang *et al* 2006), based on the error-to-signal percentage, the correlation coefficient and the evaluation of error events.

2. Methods

2.1. Data acquisition and pre-processing system

As part of the project of an active transfemoral prosthesis (figure 1(a)) (Cascão Jr *et al* 2005, Rodrigues *et al* 2006), a microcontrolled bioinstrumentation system was designed and built (figure 1(b)) using low-power consumption components (Delis *et al* 2008). The system uses INA118 front-end amplifiers with CMRR > 110 dB (Burr-Brown Corp., Tucson, AZ/Texas Instruments Inc., Dallas, TX) for SEMG signal acquisition (up to four channels) and an electrogoniometer (EMG System do Brasil Ltda, São José dos Campos, Brazil) for measuring the knee joint angle. Analog filters are used to limit the SEMG signal to the 20–500 Hz frequency range. Two channels of the amplified SEMG signal and the angle displacement signal from the electrogoniometer are analogically multiplexed and sampled using a MCP3304 13 bit analog-to-digital (ADC) converter (Microchip Technology Inc., Chandler, AZ) at a sampling rate of 1744.25 Hz (for each channel). The ADC is isolated from the power supply through an NML0505S isolated dc–dc converter (C&D Technologies Inc., Blue Bell, PA), and is optically connected to the serial peripheral interface (SPI) of an AT91SAM7S64 microcontroller (Atmel Corp., San Jose, CA) through an HCPL-2430 optocoupler (Avago Technologies Ltd, San Jose, CA).

The microcontroller implements a real-time adaptive notch filter, which maintains a running estimate of the 60 Hz power-line interference (Delis *et al* 2008). The filtered SEMG signals and the knee joint angle measurements are transferred to a personal computer through a serial interface (RS-232 C or USB) by setting the system to online mode. A block diagram of the bioinstrumentation system is shown in figure 1(c).

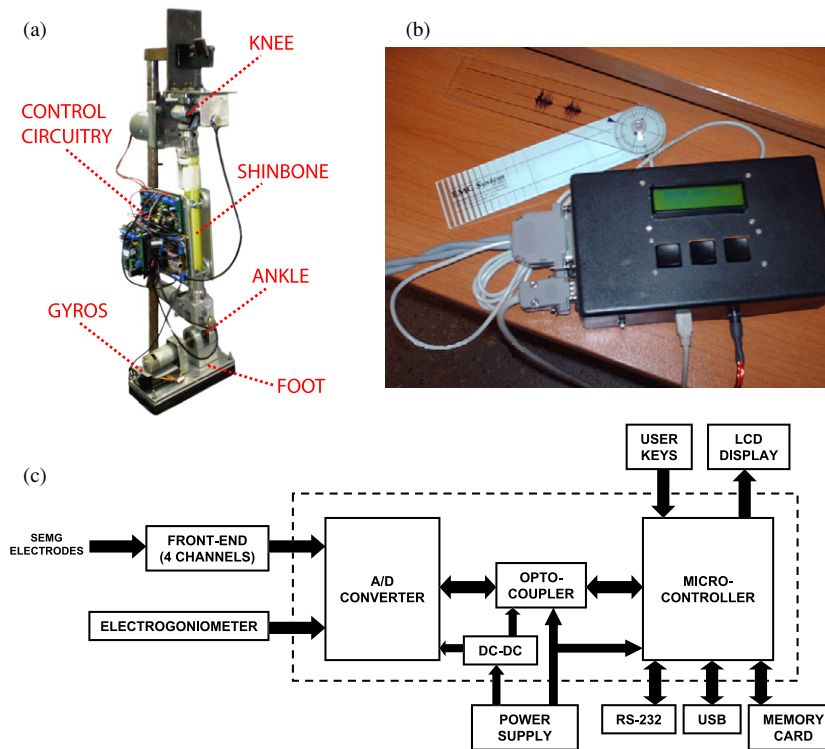


Figure 1. (a) Prosthesis prototype; (b) electrogoniometer and instrumentation system; (c) block diagram of the instrumentation system.

2.2. Subjects and the data acquisition protocol

The following experimental protocol was designed for evaluating the performance of the proposed algorithm. The protocol was approved by the research ethics committee of the University of Brasília (process no. 09/2009, group III). Four able-bodied volunteers were studied (table 1), and provided informed consent in accordance with institutional policy. Two pairs of 10 mm Ag/AgCl surface electrodes with conductive gel were placed in bipolar configuration over a pair of agonist/antagonist muscles of the same leg, corresponding to the flexion and extension movements of the knee joint, respectively (table 1 and figures 2(a) and (b)). The distance between the centers of the electrodes of each pair was 3–5 cm. Each pair of electrodes was associated with a different SEMG acquisition channel. Reference electrodes were placed over the lateralis and medialis epicondylus bones. An electrogoniometer was placed and strapped over the external side of the same leg, so that it would measure the angular displacement of the knee in sagittal plane (figure 2(c)). The two channels of SEMG data and the knee joint angle information were acquired using the bioinstrumentation system described above.

Each subject was studied over the course of 5 days. Four 10 s measurements were performed on each day, with 5 min rest periods between measurements. For each measurement, the subject was asked to walk in a particular direction at a constant pace. Some variability in pace was observed between measurements. The first and third measurements from each day were used for training, and the second and fourth measurements were used for testing. Thus,

Table 1. Age of the volunteers and corresponding experimental configurations.

| | Age | Antagonist muscles | Front-end gain |
|-----------|-----|---------------------------------------|----------------|
| Subject A | 39 | Rectus femoris and semitendinosus | 3030 |
| Subject B | 22 | Vastus intermedius and semitendinosus | 6060 |
| Subject C | 24 | Vastus lateralis and semitendinosus | 6060 |
| Subject D | 27 | Rectus femoris and semitendinosus | 6060 |

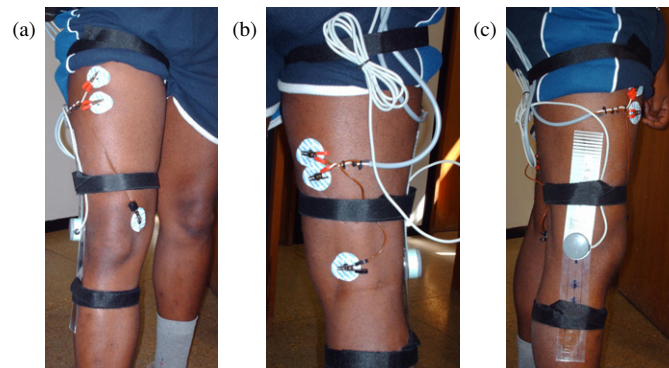


Figure 2. Placement of electrodes (a), (b) and electrogoniometer (c). The electrodes are placed in bipolar configuration over a pair of agonist/antagonist muscles, corresponding to the flexion and extension movements of the knee joint, respectively. The electrogoniometer measures the angular displacement of the knee in the sagittal plane.

a total of 80 measurements were obtained, with half of them being used for training and the other half being used for testing. Representative datasets from each volunteer are shown in figure 3.

2.3. Knee joint angle estimation algorithm

Figure 4 presents the main components of the proposed knee joint angle estimation algorithm, which is based on myoelectric pattern recognition. The proposed algorithm is composed of three main stages: (i) feature extraction, using a combination of spectral and temporal domain approaches (AR coefficients and signal amplitude histogram, respectively); (ii) feature projection, using a self-organizing map; and (iii) pattern classification, using the Levenberg–Marquardt multi-layer perceptron neural network. Feature extraction and projection is performed independently for each SEMG channel. Data from the electrogoniometer are used as reference during network training, and are not used by the network during testing. Each of these stages is discussed in detail below, followed by a discussion on the approach for training the cascade neural networks.

2.3.1. Feature extraction stage. Presenting the myoelectric signal directly to a neural classifier is impractical, because of the dimensionality and random characteristics of the signal. The signal needs to be represented by a vector of reduced dimensionality, capable of representing the signal's information in a more compact fashion. Such a vector is called a feature vector. In this work, the feature vector is composed of two sets of coefficients: the

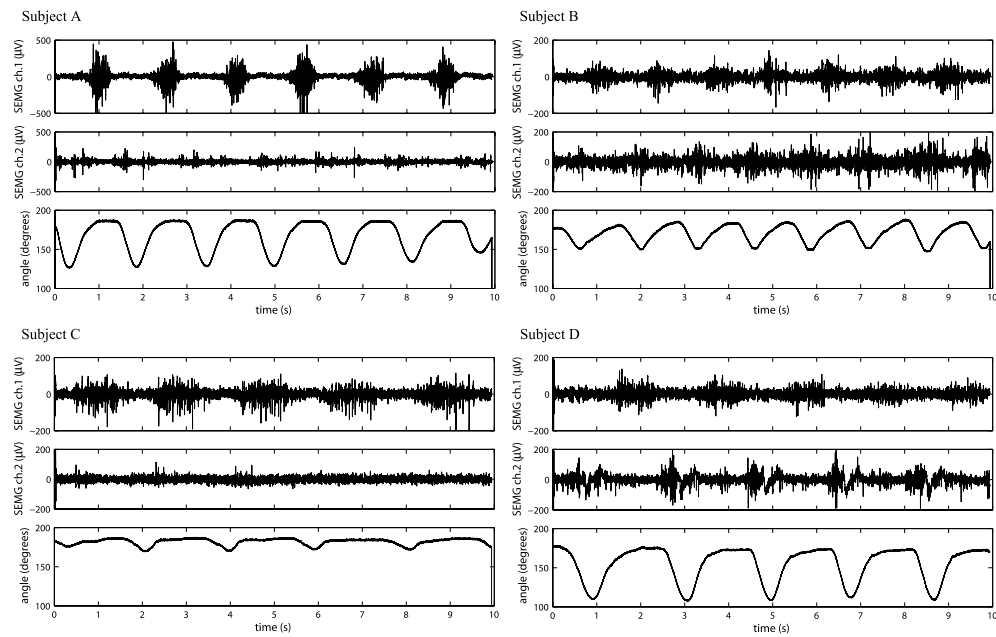


Figure 3. Representative sets of recorded SEMG signals and measured knee joint angles from each subject.

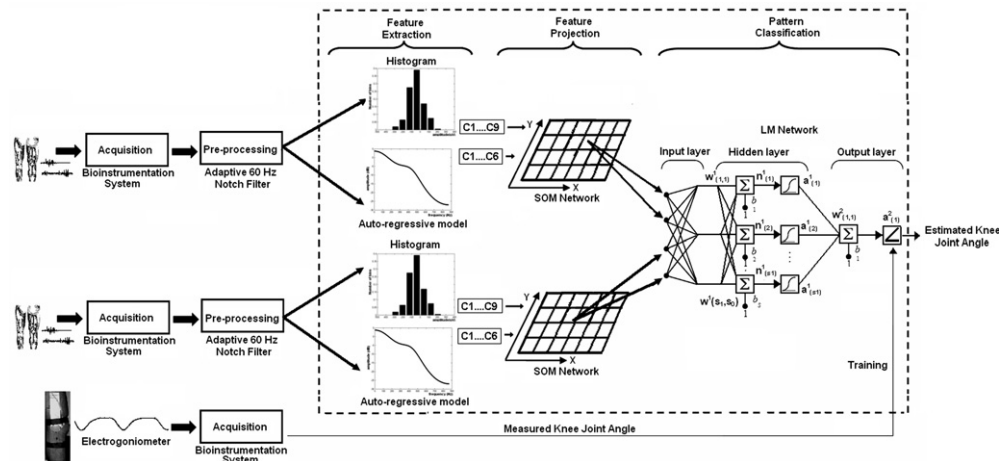


Figure 4. Block diagram of the proposed knee joint angle estimation algorithm. Feature extraction and projection is performed independently for each SEMG channel. A multi-layer perceptron neural network is used for pattern classification. Data from the electrogoniometer are used as reference only during network training, and are not used by the network during testing.

amplitude histogram bin counts, representing the time-domain characteristics of the SEMG signal, and the auto-regressive coefficients, representing the spectral content of the signal.

The SEMG amplitude histogram is an extension of the zero crossing and the Willison amplitude measures (Zardoshti-Kermani *et al* 1995). The amplitude histogram provides a

measure of the regularity in which the SEMG signal reaches each level of amplitude, associated with different histogram bins. Myoelectric signals reach relatively higher levels during the contraction period (compared to the baseline amplitude); thus, the amplitude histogram is capable of providing useful information about the state of a joint (Zardoshti-Kermani *et al* 1995). A histogram with nine symmetrically and uniformly distributed bins was used in this work. The range of values was set based on the maximum and minimum SEMG amplitude levels measured on the training datasets. The window length was set to 200 samples (115 ms).

The auto-regressive model is a convenient structure for model identification, in which the spectral envelope of the signal is modeled as an all-pole transfer function. The coefficients of this transfer function (the AR coefficients) contain information about the frequency content of the signal. In this work, the AR coefficients are used to compactly represent the spectral features of the SEMG signal (Huang *et al* 2005, Hargrove *et al* 2008). The coefficients are calculated using the recursive least-squares (RLS) algorithm with a forgetting factor (Vaseghi 2000). This gives more weight to the most recent samples at the moment of the iteration, which allows the algorithm to track temporal variations of the signal. Based on the literature (Huang *et al* 2005, Ferreira *et al* 2005) and on an evaluation using the Akaike criterion (Ljung 1987), we concluded that an AR order of 4 to 6 is sufficient to efficiently represent the SEMG signal. Thus, a sixth-order AR model was used, with a forgetting factor of 0.995, which is equivalent to 200 samples, or 115 ms.

Both the histogram window and the AR coefficients are updated for every new SEMG sample. This produces a more dense but semi-redundant stream of class decisions that could potentially be used to improve response time and accuracy (Englehart and Hudgins 2003).

2.3.2. Feature projection stage. The feature extraction stage (discussed above) reduces the dimension of the data to 15 (9 histogram bins, and 6 AR coefficients). The feature projection stage proposed in this work further reduces the dimension of the feature vector, by mapping it into a two-dimensional space using a self-organizing map.

SOM neural networks (Kohonen 2001) are trained using unsupervised learning, and are capable of arranging the input data into a discretized two-dimensional space (a map), which attempts to preserve the topological properties of the input space. The SOM is composed of nodes (or neurons). A position in the map space and a weight vector (of the same dimension as the input data vectors) are assigned to each node. The mapping algorithm consists in finding the node with the weight vector that is the closest to the input vector. The output of the SOM network is the two-dimensional coordinate of the winning node.

Each of the two SOMs (one for each SEMG channel) is arranged in a topological net with 100 neurons in their interconnection structure (10×10 matrix). The dimension of the network was chosen empirically, based on experimentation. The initial learning rate was 0.9, and the time constants τ_1 and τ_2 were 1431 and 1000 iterations, respectively (Haykin 1999). The neighborhood function initially contains all the neurons of the network, centered around the winning neuron, and with time it gradually decreases in size. Thus, the initial size of the neighborhood function is equal to the radius of the lattice (i.e. 5).

At the output of the feature projection stage, the information in each of the SEMG channels is represented by only two coefficients (a 2D coordinate), resulting in a total of four coefficients at the input of the pattern classification stage. Different coordinate pairs represent different points of operation associated with the movement of the knee joint during a walk.

2.3.3. Pattern classification stage. The pattern classification stage is responsible for providing an estimate of the knee joint angle from the set of four SOM coefficients obtained

from the feature projection stage. This is performed using a Levenberg–Marquardt multi-layer perceptron neural network (Hagan and Menhaj 1994).

There has been considerable research on methods to accelerate the convergence time of multi-layer feed-forward neural networks, such as methods that focus on standard numerical optimization techniques, including the conjugate gradient algorithm, quasi-Newton methods and nonlinear least squares (Battiti 1992, Charalambous 1992). The method used in this work is an application of a nonlinear least-squares algorithm to the batch training of multi-layer perceptrons, called the Levenberg–Marquardt algorithm. The LM algorithm is very efficient for training moderate-sized feed-forward neural networks (Hagan and Menhaj 1994). Although the computational requirements of the LM algorithm become much higher for each iteration, this is fully compensated by its higher efficiency. This is especially true when high precision is required.

The LM network used in this work has three layers in its structure, with four input nodes (output vectors of the SOM networks) in the first layer, six nodes in the second layer (associated with tangential functions) and one node in the output layer (associated with a linear function). This structure was chosen empirically, based on experiments aimed at minimizing the mean squared error (MSE). The node in the output layer represents the estimated knee joint angle (figure 4).

2.3.4. SOM and LM neural network training. The proposed algorithm was implemented and evaluated in Matlab (Mathworks, Inc., South Natick, MA). The cascade network blocks (SOM and LM) were trained independently for each set of 10 s two-channel SEMG test signals, using its corresponding set of training signals and electrogoniometer measurements.

First, the histogram and AR coefficients associated with each sample of each of the two SEMG signals were calculated. Then, these coefficients were used in the SOM networks' unsupervised training process to configure the topological map structures and set the weight vector of each neuron. Then, the same feature vectors were used in the trained SOMs, in order to generate two-dimensional vectors to be used for training the LM network.

During LM network training, the outputs from the trained SOM network were used as inputs, and the corresponding angular displacement measurements from the electrogoniometer were used as the target outputs. The same initial weight values were used for all three network layers (zero for all neurons). The maximum number of iterations was set to 50, the MSE stop criterion was 10^{-10} n.u.² and the initial learning rate was 1. These values were empirically chosen, aiming at maximum reduction of the final MSE.

2.4. Quantitative evaluation

For the validation and evaluation of performance, the proposed algorithm was quantitatively compared with the methods by Ferreira *et al* (2005) and Wang *et al* (2006).

The myoelectric algorithm by Ferreira *et al* differs from the algorithm proposed in this work by using only the AR model for feature extraction (no time-domain features), and by not using a feature projection stage. A LM network is also used as classifier.

The EWP-PCA algorithm by Wang *et al* uses time-scale feature extraction, PCA feature projection and a multi-layer perceptron neural classifier. In the feature extraction stage, the energy of the wavelet packet coefficients (EWP) was calculated by decomposing the signals to the fourth level by wavelet packet transform using the Symlet wavelet of order 5 (sym5), and then calculating the relative energy in each subspace. Then, the resulting 30-element feature vector undergoes dimensionality reduction using principal component analysis. In our implementation of this algorithm, a LM network was used for pattern classification.

For consistency with the proposed method, the same LM-network configuration was used for all three methods, and the same training process and test sets were applied. For the same reason, the wavelet decomposition in the EWP-PCA algorithm was performed for 200-sample (115 ms) windows, and a sliding-window approach was used, such that the decomposition was recalculated for every new SEMG sample. In addition, the same AR order and forgetting-factor configuration was used for the proposed method and the method by Ferreira *et al.*

The 40 sets of SEMG and electrogoniometer data which were not used for training (10 per subject) were used for comparing the three methods. The performance of each algorithm was evaluated by comparing the knee angle estimated from the SEMG signals with the angular displacement values measured with the electrogoniometer. The following metrics were used: error-to-signal percentage, correlation coefficient, and the number, amplitude and duration of error events. The Mahalanobis distance (Duda *et al* 2000) was calculated for each metric as a means of assessing the statistical difference between the proposed method and the algorithms by Ferreira *et al* and Wang *et al.*

2.4.1. Error-to-signal percentage. The error-to-signal percentage (ESP) for each test dataset was calculated using the following expression:

$$\text{ESP} = \sqrt{\frac{\sum_{i=1}^N |x(i) - \hat{x}(i)|^2}{\sum_{i=1}^N |x(i)|^2}} \times 100\%, \quad (1)$$

where $x(i)$ and $\hat{x}(i)$ are the measured and estimated knee joint angular displacements, respectively, and N is the signal length (number of samples). Then, the average ESP and standard deviation were calculated for each subject.

2.4.2. Correlation coefficient. The correlation coefficient r between two random variables x and y , with N samples and expected values \bar{x} and \bar{y} , is defined as

$$r = \frac{\sum_{i=0}^{N-1} (x_i - \bar{x})(y_i - \bar{y})}{\sqrt{\sum_{i=0}^{N-1} (x_i - \bar{x})^2 \sum_{i=0}^{N-1} (y_i - \bar{y})^2}}. \quad (2)$$

This coefficient provides a measurement of the degree of linear dependence between the two variables. It assumes values between -1 and $+1$. Negative values indicate negative correlation, positive values indicate positive correlation and $r = 0$ indicates linear independence. The closer the coefficient is to either -1 or $+1$, the stronger the correlation between the variables.

The correlation coefficient between measured and estimated knee angle displacement values for each test dataset was calculated as described above. Then, the mean and standard deviation values of r were calculated for each subject.

2.4.3. Statistics of error events. Classification errors when estimating the knee joint angle can be large or small, and also isolated or enduring. While it is obvious that large errors are more critical than small ones, it is important to note that enduring errors are more critical than isolated ones, because the system's mechanical inertia tends to filter impulse-like events. With this in mind, a metric was designed to obtain statistics on such error events, i.e. short or long series of significantly large classification errors. This metric measures the number, amplitude and duration of the error events.

The estimation error time series associated with each of the 40 test signals was calculated by taking the absolute difference between the knee joint angle measured with the electrogoniometer and the displacement angle estimated from the SEMG signals. Then,

a threshold was applied to the time series, and errors that were lower than the threshold were set to zero. This threshold was empirically set to 10° . Each series of consecutive errors found to be above the threshold was considered an error event.

From the pre-processed error time-series, the error events were segmented by (i) detecting the beginning of the event, i.e. a non-zero value found after a series of zeros, and then (ii) detecting the end of the event, i.e. a zero value found after a series of non-zero values. Then, for each event, the duration (number of samples) and maximum error amplitude were calculated. Finally, the number of error events, the maximum error event duration and the maximum error amplitude were calculated for each set of SMEG signals, and the average and standard deviation of those parameters were calculated for each subject.

2.4.4. Mahalanobis distance. The Mahalanobis distance (Duda *et al* 2000) was used for assessing the statistical difference between the proposed method and the algorithms by Ferreira *et al* and Wang *et al*. The Mahalanobis distance is a useful way of determining similarity of sample sets, as it is not dependent on the scale of measurements. For each of the above-described metrics, the Mahalanobis distance was calculated as

$$d(x, y) = \sqrt{\sum_{i=1}^N \frac{(\bar{x}_i - \bar{y}_i)^2}{\sigma_{x_i}^2 + \sigma_{y_i}^2}}, \quad (3)$$

where N is the number of subjects, \bar{x} and \bar{y} are the intra-subject means for two different algorithms, and σ_x and σ_y are the associated standard deviations. Assuming the uncertainty on \bar{x} and \bar{y} is Gaussian with zero mean, $d^2(x, y)$ follows a χ_N^2 distribution. For $N = 4$, results are considered to be statistically similar (with 95% confidence) if $d^2 \leq 9.49$, i.e. if $d \leq 3.08$.

3. Results

3.1. Training and testing

Figure 5 shows the performance of the proposed method's LM network in the course of 50 training epochs for a representative experiment. The final MSE after 50 epochs was 7.91×10^{-4} n.u.².

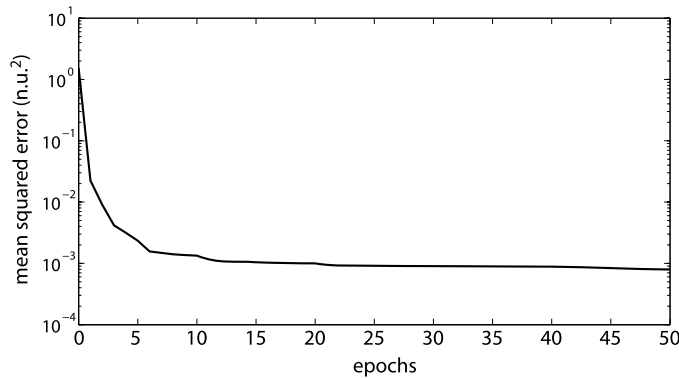


Figure 5. LM network training: MSE as a function of training epoch. The final MSE after 50 epochs was 7.91×10^{-4} n.u.² for this representative experiment.

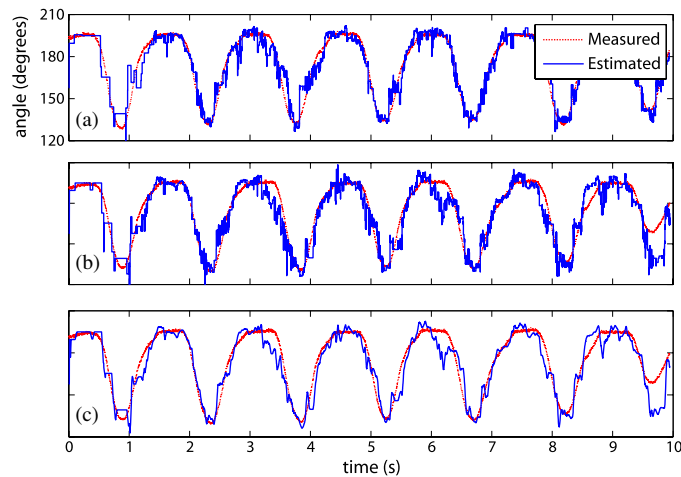


Figure 6. Measured and estimated knee joint angles for two sets of signals from the same subject: (a) training results; (b) test results; (c) filtered test results.

Figure 6 shows two time series of estimated knee joint angles from subject A, obtained during the training and testing processes, respectively. In the test results, a 50 tap (29 ms) moving average filter was used for reducing the estimation noise. Such filtering removes jitter in the output signal, which could cause undesirable and unintentional motion of the prosthesis.

3.2. Comparison with other methods

Figure 7 presents a qualitative comparison between the presented algorithm and the methods proposed by Ferreira *et al* (2005) and Wang *et al* (2006). Measured SEMG (channel 1 only) and electrogoniometer signals from two different subjects are shown (a), (e). For the acquisition of the data shown in (a), the straps holding the electrode cables were intentionally left loose, which caused movement artifacts in the SEMG signal (indicated by arrows). Measured and estimated angle displacements from each subject are shown for the algorithm by Ferreira *et al* (b), (f), the EWP-PCA method (c), (g) and the proposed algorithm (d), (h). The absolute difference between measured and estimated angles is also shown. In the presence of movement artifacts, the algorithm by Ferreira *et al* produces large errors (b). The EWP-PCA method and the proposed algorithm are more robust to such artifacts (c), (d). In the absence of movement artifacts, the method by Ferreira *et al* (f) provides lower error levels than the EWP-PCA algorithm (g). Overall, the proposed algorithm provides lower error levels than the other two methods (d), (h).

Table 2 presents the measured mean (μ) and standard deviation (σ) for the error-to-signal percentage of each subject's group of test signals, obtained with the proposed method, the algorithm by Ferreira *et al* and the EWP-PCA method. The proposed method provided lower ESP than the other two methods for all four subjects.

Table 3 presents the mean and standard deviation for the correlation coefficient of each subject's group of test signals, obtained with the proposed method, the algorithm by Ferreira *et al* and the EWP-PCA method. The proposed method provided slightly higher correlation than the algorithm by Ferreira *et al*, and considerably higher correlation than the EWP algorithm.

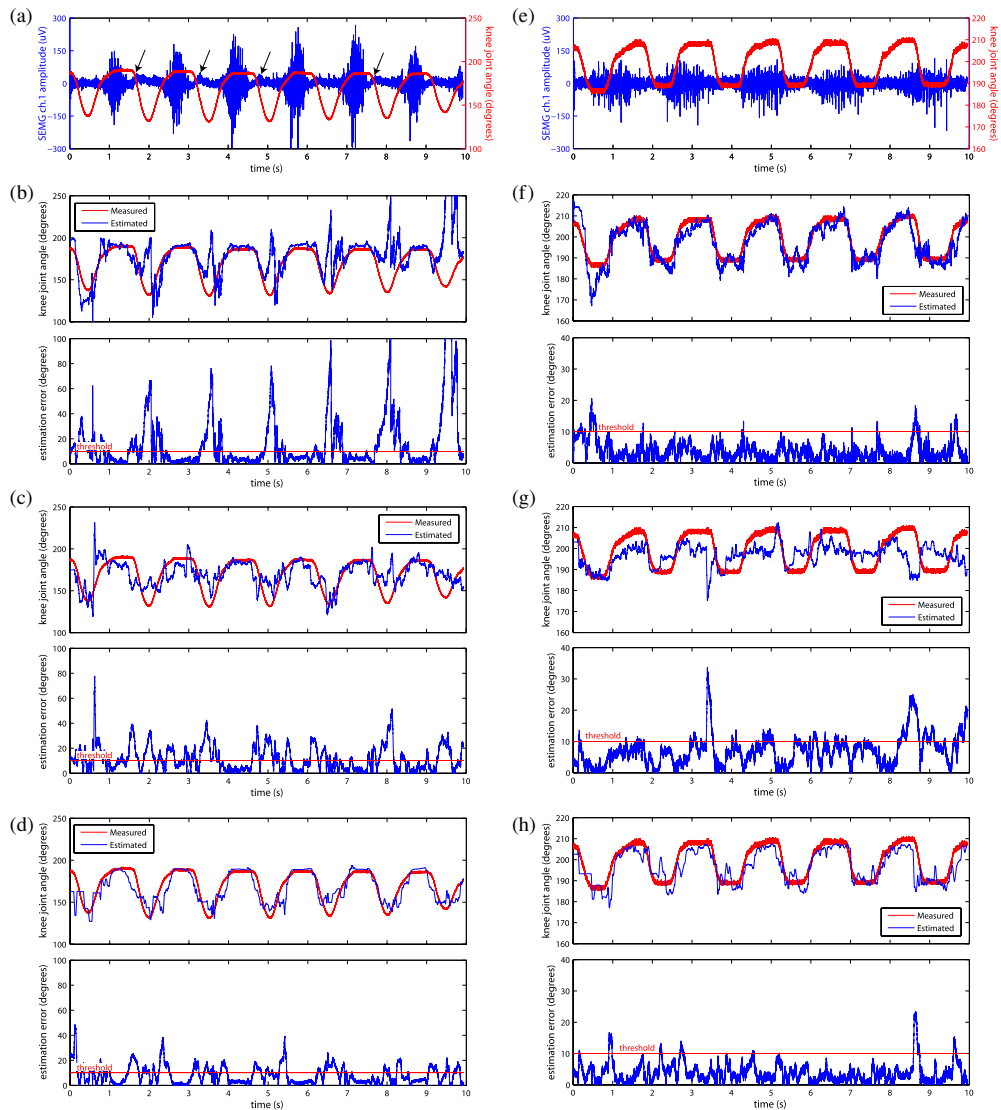


Figure 7. Qualitative comparison between the presented algorithm and the methods proposed by Ferreira *et al* and Wang *et al*. Measured SEMG and electrogoniometer signals from two different subjects are shown (a), (e). For the acquisition of the data in (a), the straps holding the electrode cables were intentionally left loose, causing movement artifacts in the SEMG signal (arrows). Measured and estimated angle displacements from each of the two subjects, and their absolute difference (estimation error), are shown for the algorithm by Ferreira *et al* (b), (f), the EWP-PCA method (c), (g) and the proposed algorithm (d), (h). The threshold level used for calculating the statistics of the error events (10°) is indicated.

Table 4 presents the average number of error events and the average maximum error event duration and amplitude (an standard deviations) found in each subject's group of test signals, for the proposed algorithm, the algorithm by Ferreira *et al* and the EWP-PCA method. The proposed algorithm provided a lower number of error events and peak error amplitude. The three methods presented equivalent maximum error event duration.

Table 2. Error-to-signal percentage, in % ($\mu \pm \sigma$).

| | Ferreira <i>et al</i> | EWP-PCA | Proposed |
|-----------|-----------------------|-----------------|-----------------|
| Subject A | 8.02 \pm 4.21 | 9.45 \pm 2.58 | 6.56 \pm 1.85 |
| Subject B | 8.18 \pm 4.70 | 7.12 \pm 1.22 | 5.33 \pm 1.13 |
| Subject C | 6.54 \pm 4.36 | 6.51 \pm 4.03 | 5.77 \pm 3.64 |
| Subject D | 6.63 \pm 3.06 | 7.54 \pm 3.17 | 5.23 \pm 1.47 |

Table 3. Correlation coefficient ($\mu \pm \sigma$).

| | Ferreira <i>et al</i> | EWP-PCA | Proposed |
|-----------|-----------------------|-----------------|-----------------|
| Subject A | 0.75 \pm 0.20 | 0.52 \pm 0.20 | 0.84 \pm 0.07 |
| Subject B | 0.54 \pm 0.27 | 0.30 \pm 0.22 | 0.61 \pm 0.22 |
| Subject C | 0.59 \pm 0.16 | 0.27 \pm 0.16 | 0.59 \pm 0.90 |
| Subject D | 0.71 \pm 0.17 | 0.34 \pm 0.19 | 0.72 \pm 0.09 |

Table 4. Statistics of error events ($\mu \pm \sigma$).

| | Number of error events | | | Maximum error event duration (ms) | | | Maximum error amplitude (degrees) | | |
|-----------|------------------------|--------------|-------------|-----------------------------------|---------------|---------------|-----------------------------------|--------------|-------------|
| | Ferreira | EWP-PCA | Proposed | Ferreira | EWP-PCA | Proposed | Ferreira | EWP-PCA | Proposed |
| Subject A | 45 \pm 10 | 252 \pm 64 | 27 \pm 5 | 433 \pm 154 | 441 \pm 82 | 450 \pm 206 | 76 \pm 48 | 98 \pm 67 | 42 \pm 11 |
| Subject B | 71 \pm 15 | 240 \pm 71 | 32 \pm 11 | 398 \pm 105 | 385 \pm 71 | 377 \pm 187 | 61 \pm 49 | 161 \pm 48 | 30 \pm 7 |
| Subject C | 34 \pm 11 | 181 \pm 63 | 18 \pm 6 | 719 \pm 442 | 500 \pm 293 | 691 \pm 512 | 47 \pm 27 | 158 \pm 69 | 29 \pm 12 |
| Subject D | 51 \pm 12 | 192 \pm 44 | 28 \pm 8 | 413 \pm 183 | 400 \pm 160 | 339 \pm 132 | 49 \pm 36 | 130 \pm 71 | 33 \pm 11 |

Table 5. Mahalanobis distance between the proposed method and the algorithms by Ferreira *et al* and Wang *et al*, for each of the evaluated metrics.

| | Proposed versus Ferreira <i>et al</i> | Proposed versus EWP-PCA |
|------------------------------|---------------------------------------|-------------------------|
| Error-to-signal percentage | 0.80 | 1.56 |
| Correlation coefficient | 0.48 | 2.58 |
| Number of error events | 3.34 | 6.38 |
| Maximum error event duration | 0.35 | 0.44 |
| Maximum error amplitude | 1.19 | 3.63 |

Table 5 presents the measured Mahalanobis distance between the proposed method and the algorithms by Ferreira *et al* and Wang *et al*, respectively, for each of the five metrics shown in tables 2, 3 and 4. When compared with the algorithm by Ferreira *et al*, the proposed method achieved a statistically significant reduction in the number of error events. When compared with the EWP-PCA algorithm, the proposed method achieved a statistically significant reduction in the number of error events and maximum error amplitude. Results were considered statistically significant for $d > 3.08$ (see section 2.4.4).

4. Discussion

The presented method is proposed as an improvement to the algorithm by Ferreira *et al* (2005). The most important modification is the addition of a feature projection stage—a SOM network—to the system. The addition of the amplitude histogram to the feature extraction stage also plays an important role in the algorithm, as the combination of temporal and spectral features is known to improve the robustness to electrode displacement (Hargrove *et al* 2008). Such improvement was observed in some of the signals obtained from one of the subjects (figures 7(a)–(d)).

The proposed method achieved better results than the algorithms by Ferreira *et al* and Wang *et al* for all the quantitative metrics used in this work, except for the duration of error events (table 4). One possible reason is noise in the feature space (AR and histogram coefficients). While the feature projection stage is able to reduce the amplitude of such variations, their duration may remain unchanged.

The maximum error amplitudes measured with the proposed method are considerably reduced when compared to the results using the other two algorithms; however, they are still large (table 4). Nevertheless, this may not be a significant issue, as short duration error events are unnoticeable to the leg prosthesis, due to the system's mechanical inertia. These short duration error peaks may be caused due to noise in the feature space, and/or by an insufficient number of neurons in the SOM network and in the LM network's hidden layer. This problem may be addressed by increasing the number of neurons, by increasing the number of SEMG signals and/or adding other variables associated with leg proprioception (e.g. accelerometers). These approaches would result in increased computational network complexity and convergence time. Alternatively, error peaks may be avoided by increasing the forgetting factor of the AR/RLS algorithm and the window length of the histogram. However, this approach would increase the response time of the prosthesis.

The accuracy of the proposed method in the presence of transient data may be improved using time-frequency and time-scale feature projection (e.g. wavelets, short-time Fourier transform) (Englehart *et al* 2001). However, these approaches are more computationally intense than the combination of AR coefficients with an amplitude histogram, as proposed in this work, and would also affect the networks' complexity. Furthermore, time-domain and AR features have been shown to outperform time-frequency features for stationary or slowly changing data, and to provide equivalent results for steady-state SEMG signals (Huang *et al* 2005).

One important aspect to consider when designing systems for estimation of user motion intention based on physiological measurements is overtraining. It is expected that the validity of the trained models is limited only to a given period of time. Such period may be made shorter due to overtraining. In all methods investigated in this paper, the performance is not expected to be sustained for days, or even for a few hours. This motivates the use of other type of sensors on the prosthesis, which may potentially allow parameter adaptation during the use of the prosthesis by the patient. For example, microelectromechanical gyroscopes and joint motion sensor may be used for measuring the angular velocity of the knee joint. The integration of these data can be used to obtain an estimate of the knee joint angle, which can be used to make small corrections of the neural network coefficients in real time.

5. Conclusion

This work introduces an algorithm for knee joint angle estimation from SEMG signals, which may be used for myoelectric control of transfemoral leg prostheses. The proposed method

improves the algorithm originally presented by Ferreira *et al* (2005), by adding a feature projection stage (a SOM network) and by incrementing the feature extraction stage with a signal amplitude histogram. Feature extraction now combines time-domain (histogram) and frequency-domain (AR coefficients) features. Pattern classification is still performed using a Levenberg–Marquardt multi-layer perceptron neural network, but this is now more efficient due to the dimensionality reduction provided by the SOM network.

The improved method was quantitatively compared with the original algorithm and with the EWP-PCA method. The proposed algorithm presented higher correlation, lower error-to-signal ratio and peak error amplitude, and fewer error events.

We have shown that it is possible to continuously decode knee position from SEMG signals collected from a generalized electrode placement in an able-bodied subject. Future work will be aimed at (i) reducing noise, (ii) evaluating the method in amputees, (iii) optimizing the code for its execution in real time, and (iv) adding accelerometer sensors and adaptive Kalman filtering to the system. The latter will not only improve the system's accuracy at estimating the knee joint angle, but also allow the myoelectric control algorithm to estimate the angular velocity of displacement of the knee joint.

Acknowledgments

This work was financially supported by a grant from the Brazilian Ministry of Education—MEC/CAPES—and by a doctoral fellowship from the National Council for Technological and Scientific Development—CNPq (to ALD).

References

- Battiti R 1992 First and second order methods for learning: between steepest decent and Newton's method *Neural Comput.* **4** 141–66
- Cascão C A Jr, Ferreira R U, Beckmann E D, Borges G A, Ishihara J Y and da Rocha A F 2005 Estudo e desenvolvimento de uma prótese ativa de perna comandada por sinais eletromiográficos *Proc. VII Simpósio Brasileiro de Automação Inteligente/II IEEE Latin-American Robotics Symp. (São Luís, Brazil, 18–23 September 2005)*
- Charalambous C 1992 Conjugate gradient algorithm for efficient training of artificial neural networks *IEE Proc. G* **139** 301–10
- Chu J U, Moon I, Kim S K and Mun M S 2005 Control of multifunction myoelectric hand using a real time EMG pattern recognition *Proc. IEEE/RSJ Int. Conf. Intelligent Robots and Systems (Edmonton, Canada, 2–6 August 2005)* pp 3957–62
- Delis A L, da Rocha A F, dos Santos I, Sene I G Jr, Salomoni S and Borges G A 2008 Development of a microcontrolled bioinstrumentation system for active control of leg prostheses *Proc. 30th Ann. Int. Conf. Engineering in Medicine and Biology Society (Vancouver, Canada, 20–24 August 2008)* pp 2393–96
- Duda R O, Hart P E and Stork D G 2000 *Pattern Classification* 2nd edn (New York: Wiley)
- Englehart K and Hudgins B 2003 A robust, real time control scheme for multifunction myoelectric control *IEEE Trans. Biomed. Eng.* **50** 848–54
- Englehart K, Hudgins B and Parker P A 2001 A wavelet-based continuous classification scheme for multifunction myoelectric control *IEEE Trans. Biomed. Eng.* **48** 302–10
- Ferreira R U, da Rocha A F, Cascão C A Jr, Borges G A, Nascimento F A O and Veneziano W H 2005 Reconhecimento de padrões de sinais de EMG para controle de prótese de perna *Proc. XI Congresso Brasileiro de Biomecânica (João Pessoa, Brazil, 19–22 June 2005)*
- Fukuda O, Tsuji T, Kaneko M and Otsuka A 2003 A human-assisting manipulator teleoperated by EMG signals and arm motions *IEEE Trans. Robot. Autom.* **19** 210–22
- Hagan M T and Menhaj M B 1994 Training feedforward networks with the Marquardt algorithm *IEEE Trans. Neural Netw.* **5** 989–93
- Hargrove L, Englehart K and Hudgins B 2008 A training strategy to reduce classification degradation due to electrode displacements in pattern recognition based myoelectric control *Biomed. Signal Process. Control* **3** 175–80

- Haykin S 1999 *Neural Networks: A Comprehensive Foundation* 2nd edn (Englewood Cliffs, NJ: Prentice-Hall)
- Huang Y, Englehart K, Hudgins B and Chan A D C 2005 A Gaussian mixture model based classification scheme for myoelectric control of powered upper limb prostheses *IEEE Trans. Biomed. Eng.* **52** 1801–11
- Hudgins B, Parker P A and Scott R N 1993 A new strategy for multifunction myoelectric control *IEEE Trans. Biomed. Eng.* **40** 82–94
- Kelly M F, Parker P A and Scott R N 1990 The application of neural networks to myoelectric signal analysis: a preliminary study *IEEE Trans. Biomed. Eng.* **37** 221–30
- Kohonen T 2001 *Self-Organizing Maps* 3rd edn (New York: Springer)
- Ljung L 1987 *System Identification: Theory for the User* (Englewood Cliffs, NJ: Prentice-Hall)
- Liu Y H, Huang H P and Weng Ch H 2007 Recognition of electromyographic signals using cascade kernel learning machine *IEEE/ASME Trans. Mechatronics* **12** 253–64
- Monseni-Bendpei M A, Watson M J and Richardson B 2000 Application of surface electromyography in the assessment of low back pain: a literature review *Phys. Ther. Rev.* **2** 93–105
- Rodrigues S S, Ferreira R U, Marques Junior M F, Beckmann E D, Santos G F, Borges G A, Ishihara J Y and da Rocha A F 2006 Estudo e desenvolvimento de uma prótese robótica de perna comandada por sinais eletromiográficos *Proc. IV Congresso Ibero-Americano Sobre Tecnologias de Apoio a Portadores de Deficiência (Vitória, Brazil, 20–22 February 2006)*
- Smith R J, Tenore F, Huberdeau D, Etienne-Cummings R and Thakor N V 2008 Continuous decoding of finger position from surface EMG signals for the control of powered prostheses *Proc. 30th Ann. Int. Conf. Engineering in Medicine and Biology Society (Vancouver, Canada, 20–24 August 2008)* pp 2393–6
- Sommerich C M, Joines S M, Hermans V and Moon S D 2000 Use of surface electromyography to estimate neck muscle activity *J. Electromyogr. Kinesiol.* **6** 377–98
- Vaseghi S V 2000 *Advanced Digital Signal Processing and Noise Reduction* 2nd edn (New York: Wiley)
- Wang G, Wang Z, Chen W and Zhuang J 2006 Classification of surface EMG signals using optimal wavelet packet method based on Davies–Bouldin criterion *Med. Biol. Eng. Comput.* **44** 865–72
- Zardoshti-Kermani M, Wheeler B C, Badie K and Hashemi R M 1995 EMG feature evaluation for movement control of upper extremity prosthesis *IEEE Trans. Rehabil. Eng.* **3** 324–33
- Zhao J, Xie Z, Jiang L, Cai H, Lio H and Hirzinger G 2006 EMG control for a five-fingered interactuated prosthetic hand based on wavelet transform and sample entropy *Proc. IEEE/RSJ Int. Conf. Intelligent Robots and Systems (Beijing, China, 9–15 October 2006)* pp 3215–20